GEOLOGOS

Shock veins in the Sahara 02500 ordinary chondrite

Krzysztof Owocki[1] & Andrzej Muszyński[2]

[1]Institute of Paleobiology, Polish Academy of Sciences, Twarda 51/55, 00-818 Warsaw, Poland;
e-mail: kowoc@twarda.pan.pl

[2]Institute of Geology, Adam Mickiewicz University, Maków Polnych 16, 61-606 Poznań, Poland;
e-mail: anmu@amu.edu.pl

Abstract

A specimen of the Sahara 02500 ordinary chondrite contains shock-produced veins consisting of recrystallised fine-grained pyroxenes that include small droplets of Ni-rich metal. Non-melted olivines and pyroxenes show planar deformations filled by shock-melted and -polluted metal and troilite. Shock-melted feldspathic glass is present close to the shock veins. Geothermometric estimations indicate that the meteorite locally experienced moderate shock metamorphism with a minimum local peak temperature above 1400ºC, resulting in partial melting of Ca-poor pyroxene and full melting of feldspars, metal and sulphides. The mineral assemblage in the shock veins suggests a pressure during melt recrystallisation below 10 GPa.

Keywords: ordinary chondrite, shock veins, subsolidus recrystallization

1. Introduction

Shock metamorphism causes widespread textural changes in chondritic meteorites; in the case of the highest shock levels, also mineralogical changes take place, including the formation of new high-pressure phases such as ringwoodite or perovskite. Shock effects are commonly heterogeneous, resulting in the partial melting of some parts of the meteorite, producing shock veins and melt pockets (Brearley & Jones, 1998). Recently, many petrologists and planetologists focus on the mineralogy of shock veins and melt pockets, using them to estimate the shock pressure (e.g. Xie et al., 2006) in meteorites – an alternative tool to the Stoffler et al. (1991) scheme based on shock effects in olivine and plagioclase.

Most works focus, however, on high-pressure phases (Chen et al., 2004; Ohtani et al., 2004; Xie et al., 20011) and impact-melt breccias (e.g. Rubin, 2002), neglecting meteorites which have shock veins with a more robust mineralogy. Here we present detailed observations of the microstructure and mineral assemblage in shock-induced melt veins found in the Sahara 02500 ordinary chondrite. The crystallisation pressure and temperature constraints and the cooling rate were inferred from the melt-vein mineralogy and compared with published data from other meteorites.

2. Analytical techniques

A thin section was prepared from a small chip of the Sahara 02500 meteorite and analysed in polarised light with an optical microscope (NICON Eclipse LV 100 POL). Backscattered electron images, chemical analyses and maps were obtained using a Cameca SX-100 Electron Micro Probe (Joint-Institute Analytical

Complex for Minerals and Synthetic Substances, Warsaw) and a Hitachi S–3700N scanning electron microscope (Didactical Workshop of Scanning Microscopy and Microanalysis, Faculty of Geographical and Geological Sciences, Adam Mickiewicz University, Poznań).

The microprobe was used for carbon-coated polished thin sections under the following conditions: an accelerated voltage of 15 kV, a beam current of 20 nA and a beam spot of 1.5 μm. Well-defined minerals and synthetic phases were used as standards. The peak counting times were 10 s for major elements and 20 s for minor elements. At these durations, the average detection limits were 0.017–0.03 wt% for Ca, Mg, Si, Al, Zn and V; they were 0.03–0.05 wt% for Cr, Na, K, Ti, P; and 0.06–0.1 wt% for Fe, Mn, Ni, Co, F and Cl.

The Raman spectra measurements were performed at the Laboratory of Intermolecular Interactions, Faculty of Chemistry, Warsaw University. Raman point analyses were performed with a LabRAM HR800 (Horiba Jobin Yvon) spectrometer, coupled with an Olympus BX61 confocal microscope. The instrument was equipped with a Peltier-cooled CCD detector (1024 × 256 pixels). The measurements were carried out utilizing a diode-pumped, frequency-doubled Nd:YAG laser (532 nm, P_{max} = 100 mW on the head). Spectra were collected in a backscattering configuration, using a 100× magnification Olympus objective. The confocal pinhole size was set to 200 μm and the calibration of the instrument was performed utilizing a 520 cm^{-1} Raman signal from a silicon wafer.

All Raman spectra were collected using a filter reducing the power of the laser beam on the sample to 0.25–0.30 mW. Spectra were taken from three shock-vein areas at different locations. Two sets of Stokes spectra with a 15-μm lateral resolution were acquired. The Raman spectra were obtained and analysed using LabSpec5 software.

3. Petrology and mineralogy

The specimen under study has a mass of 20 g. It has a characteristic thin, dark brown fusion-crust. In thin section, the specimen is light-grey and its chondrules are recrystallised but retain well-defined boundaries (Fig. 1 A-C). The chondrules are predominantly of a porphyritic type (porphyritic olivine, porphyritic olivine-pyroxene and bared olivine type); 10% of the chondrules are radial pyroxene chondrules. Cryptocrystalline chondrules are not present. The chondrule mesostasis is crystalline; only a few chondrules show a turbid mesostasis. In thin section, L6 clasts (Fig. 1B) account for about 10% (vol) of the meteorite. Metals and sulphides are present in the specimen as fine-grained disseminated inclusions with a regular or amoeboid shape.

The chondrules and the crystalline matrix are composed predominantly of olivine, with smaller amounts of ortho- and clinopyroxene. The olivines have an equilibrated composition (Fo 75.20% mol; Fa 24.44% mol) with a low content of TiO_2 and Cr_2O_3 (below 0.1% wt). The Ca-poor pyroxene has a well-equilibrated average composition (Wo 1.85% mol; En 77.78% mol; Fs 20.35% mol). The mean Fe/(Fe+Mg) ratio is higher in the olivine (24.91) than in the Ca-poor pyroxene (20.74). Minor and accessory phases include pigeonite, Ca-rich pyroxenes with augite>diopside (vol), phosphates (merrillite and Cl-apatite) and feldspar (Ab 87.59 mol%, Or 2.87 mol%, An 9.53 mol%) with maximum sizes of 5 μm. Kamacite, taenite and troilite are present as tiny amoeboid inclusions (3% vol in thin section).

The olivine and Ca-poor pyroxene compositions are within the range of L-chondrites. The well-defined chondrule boundaries, the turbid to crystalline chondrule mesostasis, the small feldspar grains and the presence of L6 clasts suggest that the Sahara 02500 meteorite is a type 4–6 geomict breccia according to the classification of Van Schmus & Wood (1967). The planar deformation fractures and the weak mosaicism in olivine (Fig. 1 C-D), as well as the presence of shock veins all indicate that the meteorite has been moderately shocked after metamorphism. According to the classification scheme of Stoffler et al. (1991), the shock stage is estimated to be S4 (moderately shocked).
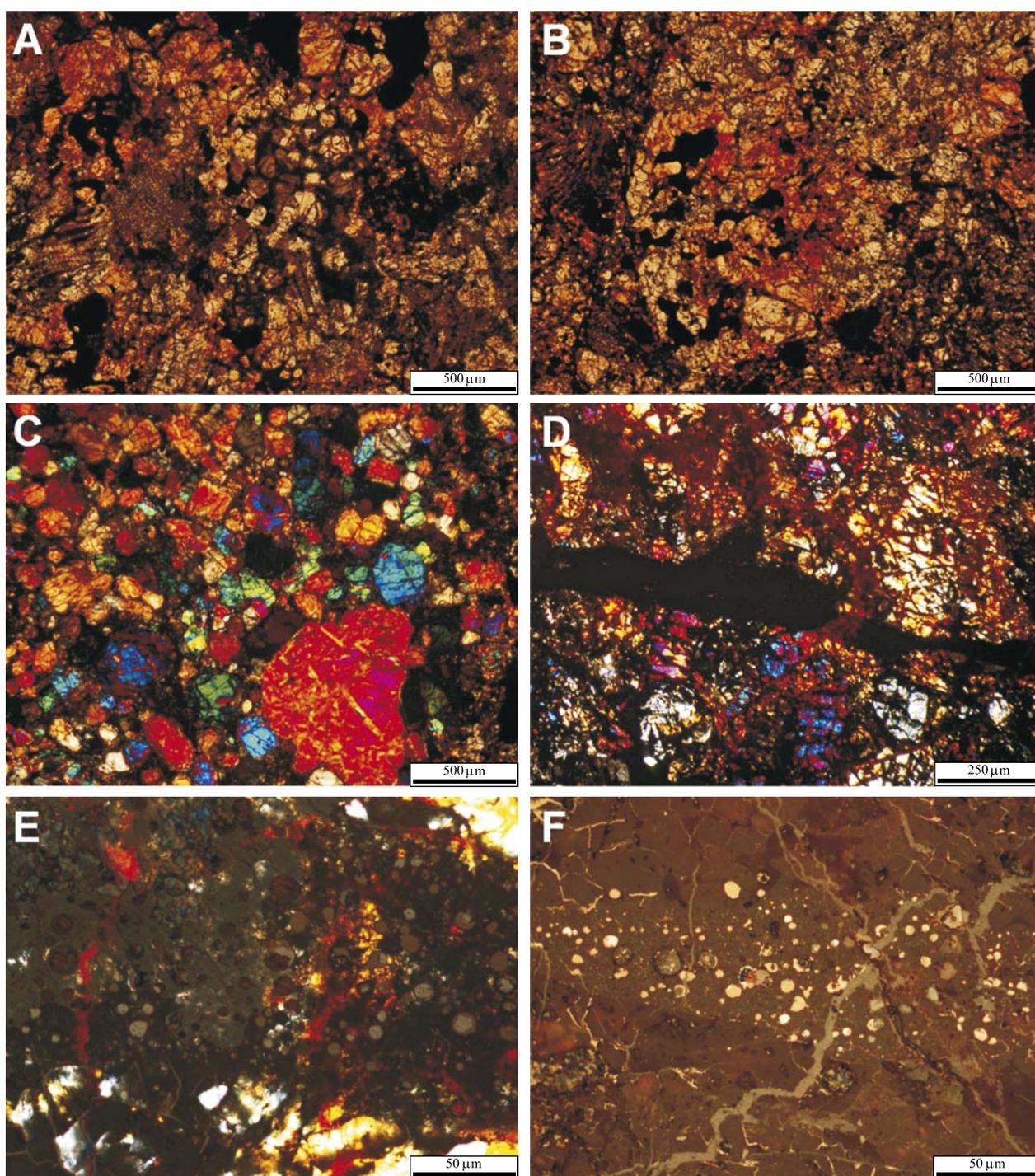
Fig. 1. Details of the Sahara 02500 meteorite (A-B and E transmitted light IIP, C-D transmitted light XP, F-reflected light IIP).
A-C: Structure and texture (note the L6 clast in Fig. 1B); **D:** Shock vein and shock-darkened surroundings; **E-F:** Structure of the shock vein.

4. Shock veins

About 10% of the meteorite is darkened and translucent in transmitted light. Low-resolution microphotography shows that this area consist of mineral grains with a dense network of planar deformation features, highlighted by opaque material (Fig. 1 D). Reflected-light observations and EMP analyses show that these features are filled with troilite and its weather-
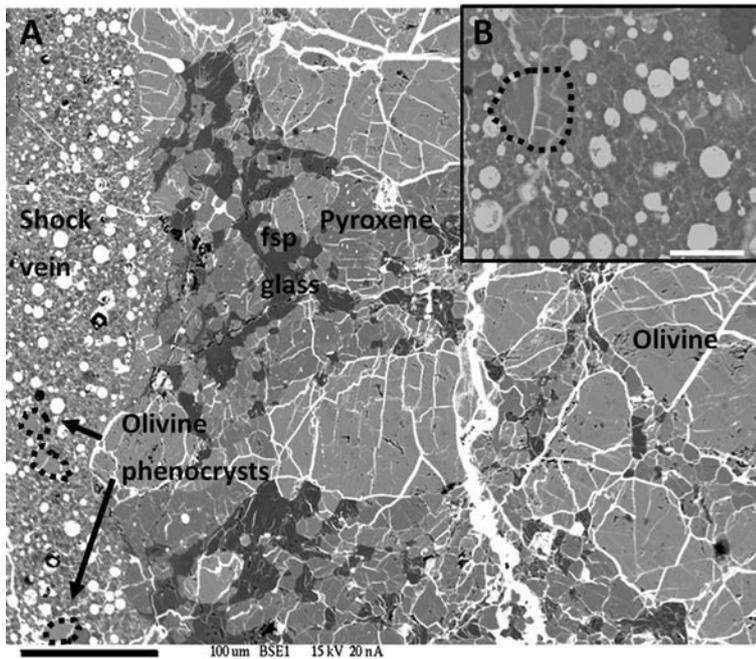
Fig. 2. Back-scattered electron micrograph of the mapped area of the shock vein in Sahara 02500. Note the feldspathic glass, the Ni-rich metal in PDF's, and the shock-vein blebs. Scale bar Fig. A: 100 μm; B: 20 μm.

ing products, and that they are responsible for the silicate darkening around the shock veins (cf. Rubin, 1992).

Two types of shock features are present in the sample under examination. the first type are shock-induced melt veins and pockets that contain silicates (Fig. 1 D-F) and the second type are iron-oxide veins which cross-cut melt veins and represent weathering of metal-sulphide veins that postdate the silicate melt veins. the small melt pockets are connected with the shock veins and will be further referred to as 'veins' because they have the same texture and composition. Moreover we could observe these features only in the planar sections and we do not know how their spatial relations are outside this plane.

Low-resolution BSE images (Fig. 2) show that the veins have variable thicknesses, from 10 to 120 μm, although some parts reach 250–500 μm. The texture of the veins is uniform, with a microcrystalline silicate matrix surrounding blebs of metal-troilite (Table 1) and host-rock fragments. The blebs are well rounded and have variable diameters of 3–20 μm (mean 12 μm); they are embedded in the fine-grained silicate matrix with crystallites of less than 1 μm. Element maps (Fig. 3) show that the host-rock fragments are usually olivine grains with a diameter varying between 10 and 35 μm, whereas the surrounding vein silicates have an Mg content similar to that of the pyroxenes adjacent to the vein.

Table 1. Analyses by electron microprobe (wt%) of metals and sulphides in the shock veins in the Sahara 02500 meteorite. For kamacite and troilite only analyses totalling 97–102 wt% are presented.

	oxidized vein	troilite	troilite	oxidized vein	kamacite	kamacite	kamacite
Si	0.86	0.04	0.09	0.03	0.04	0.05	0.08
P	0.02	0.01	0.01	0.01	0.01	b.d.l.	0.06
S	0.21	34.77	35.17	0.06	0.06	0.05	0.01
Fe	53.55	62.34	62.98	86.42	96.08	95.99	96.29
Ni	4.42	0.22	0.45	2.55	2.54	2.50	2.85
Co	0.36	0.04	0.03	0.68	0.92	0.81	0.81
total	59.42	97.42	98.73	89.75	99.65	99.40	100.10

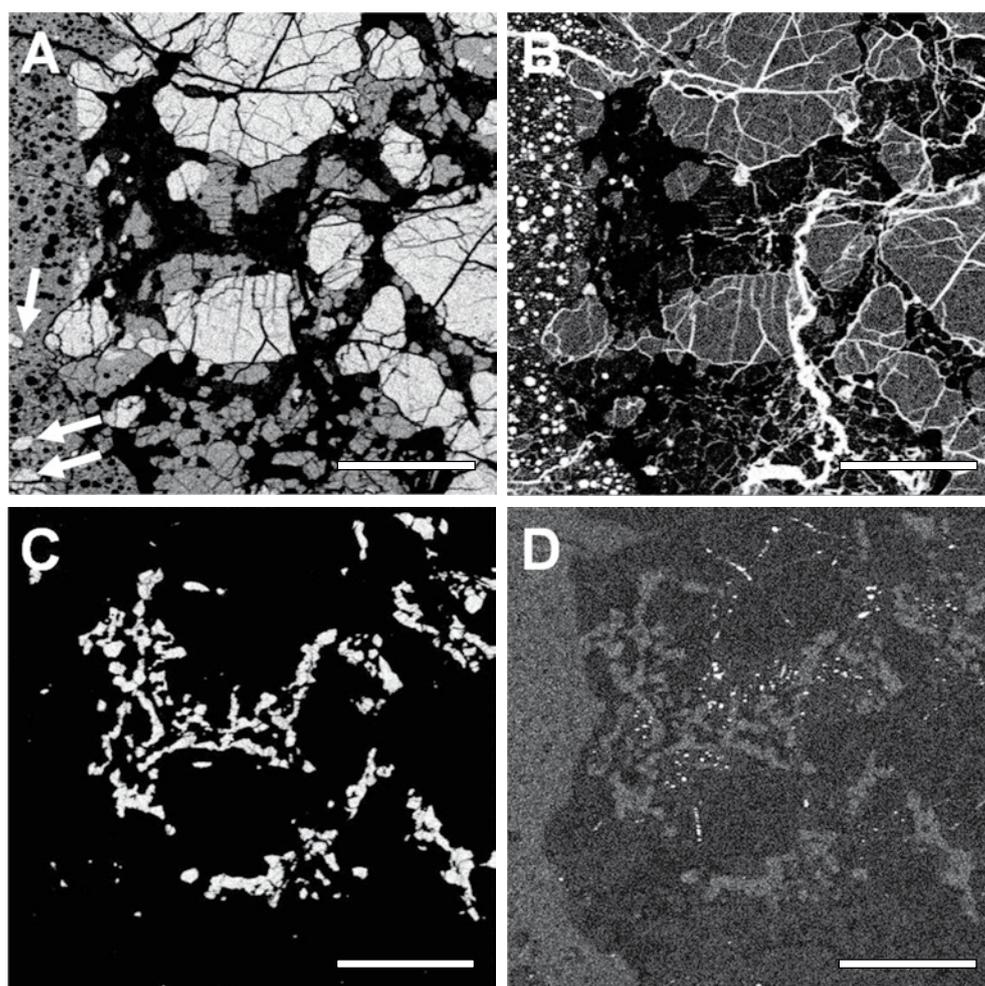b.d.l. = below detection limit

Fig. 3. Element map of the melts in Sahara 02500 (from upper left to lower right: Mg, Fe, Ca, Cr). Note the olivine phenocrysts (arrowed). Scale bars 100 μm.

The homogeneity of the texture suggest that crystallisation occurred after pressure release, and the presence of well rounded metal-troilite blebs indicates that the veins reached temperatures that were high enough to form immiscible silicate and metal-sulphide melts.

Raman spectroscopy was used to determine the composition of the silicates in the melt veins. A characteristic double peak at the 820–852 cm^{-1} wave number region of the spectrum (Fig. 4) was identified as olivine (olivine phenocryst embedded in shock vein and randomly caught by a analyzing laser beam), with second-order peaks at 952 cm^{-1} and 916 cm^{-1}. The first-order wave bands at 666 cm^{-1} and 1011 cm^{-1} and the second-order peaks at 536–578 cm^{-1} were identified as clinopyroxene.

The Raman data are consistent with EMP spot analyses (Table 2) showing a pyroxene composition of En 60–80% mol, Fs 15–36% mol and Wo 1.6–3.6% mol. The EMP data are inaccurate, however, as melt-vein silicates have crystallites that are much smaller than the electron beam used by the analytical instrument.

The BSE investigations showed that some opaque phases adjacent to the shock veins consist of igneous feldspathic glass. This glass contains numerous inclusions (Table 2) and its CaO content decreases in the direction towards the shock veins, whereas the content of Na_2O and K_2O increases. Both the glass and the shock-vein silicates show a uniform distribution of Cr (Fig. 3), suggesting rapid cooling of the melts produced by the shock event.

Table 2. Analyses by electron microprobe (wt%) of the fine grained silicate phases in the shock veins in the Sahara 02500 meteorite. Only analyses totalling 90–110 wt% are presented.

	px	px	px	px	px	olivine phenoc-ryst	olivine phenoc-ryst	fsp glass	fsp glass	fsp glass
K_2O	0.81	1.12	0.35	n.m.	0.15	0.73	1.04	3.57	4.65	4.02
CaO	2.01	2.23	1.61	21.66	1.79	1.84	1.58	1.81	1.71	1.57
TiO_2	0.13	0.08	0.07	0.48	0.04	0.17	0.14	0.03	b.d.l.	b.d.l.
Cr_2O_3	0.27	0.32	0.51	0.97	0.48	0.80	0.60	n.m.	n.m.	n.m.
P_2O_5	0.23	0.24	0.11	b.d.l.	0.10	0.24	0.55	0.02	n.m.	n.m.
Fe_2O_3	15.66	14.92	14.17	6.12	9.55	27.81	22.89	0.72	0.41	2.15
MnO	0.32	0.22	0.38	0.14	0.20	0.46	0.52	0.07	n.m.	n.m.
ZnO	b.d.l.	0.03	0.02	b.d.l.	b.d.l.	0.04	b.d.l.	0.01	b.d.l.	b.d.l.
Na_2O	0.54	1.76	1.88	0.56	0.73	0.59	0.66	4.90	6.69	4.93
MgO	23.96	22.56	30.59	15.94	28.80	25.49	25.47	0.23	n.m.	n.m.
Al_2O_3	4.46	5.12	2.00	0.51	2.95	3.37	4.28	22.75	22.03	19.92
SiO_2	48.02	47.88	41.72	54.15	54.80	41.10	44.13	71.07	67.04	63.01
total	96.41	96.48	93.41	100.53	99.59	102.64	101.86	105.18	102.53	95.60

px = pyroxene, fsp = feldspathic; n.m. = not measured, b.d.l. = below detection limit

5. Discussion

A plagioclase phase diagram at 1 atm (McDuff & Heath, 2001) has been used to determine the peak temperatures of the solidification of the feldspathic glass, which turn out to vary between 1370°C and 1118°C. For the micro-granular pyroxene, an Fe/(Fe+Mg) vs. Ca/(Ca+Fe+Mg) geothermometer (Putirka, 2005) and a meteorite pyroxene geothermometer (Lindley, 1983) were used to determine the crystallisation temperatures of the pyroxene melt in the shock veins, which indicated solidus temperatures around 850°C. A solid-state Fe-Ni phase diagram (Yang et al., 1997) shows a taenite equilibrium at 490°C.

High-temperature experiments (Bogert et al, 2003) and petrological examination of fission crusts of ordinary chondrites (McSween et al., 1978) suggest that few seconds of intense heating are sufficient to cause troilite to melt and fill delicate fractures as observed in the examined specimen. The presence of metal-troilite blebs in the shock veins indicates that the shock temperature was above the Fe-FeS eutectic temperature of 988°C (Rubin, 2002).

The melt pocket in the Sahara 02500 meteorite reflects two stages of cooling, which is characteristic for an impact melt. At first a superheated impact melt thermally equilibrates with cooler clastic material. Later the sub-solidus breccias of the melt and the clasts cool more slowly. It is possible to determine the rate of the initial cooling with the method of Scott (1982) by examining the nucleation and growth of metal particles in the melt. The faster the cooling takes place, the less metal particles form and the greater the distance between them. Based on 60 spacings that ranged from 5 to 20 µm, we determined the cooling rate to have been ~846±60 K/s.

The experiments by Bogert et al. (2003) showed that the presence of melt veins and darkening does not imply that an ordinary chondrite has undergone severe shock deformation. In fact, quick strain-induced deformation and frictional melting are responsible for shock veins at low shock pressures (Bogert et al., 2003). Xie et al. (2006) analyzed shock veins in seven L chondrites and suggest that the Stoffler et al. (1991) classification is too high by a factor of 2 for S6 samples

In order for high-pressure phases such as perovskite to have survived in the melt vein, the melt vein temperature must have been below the breakdown temperature before the shock pressure was released and fast cooling occurred. The relatively fast cooling calculated above and the presence of pyroxene instead of perovskite suggest that in the case of Sahara
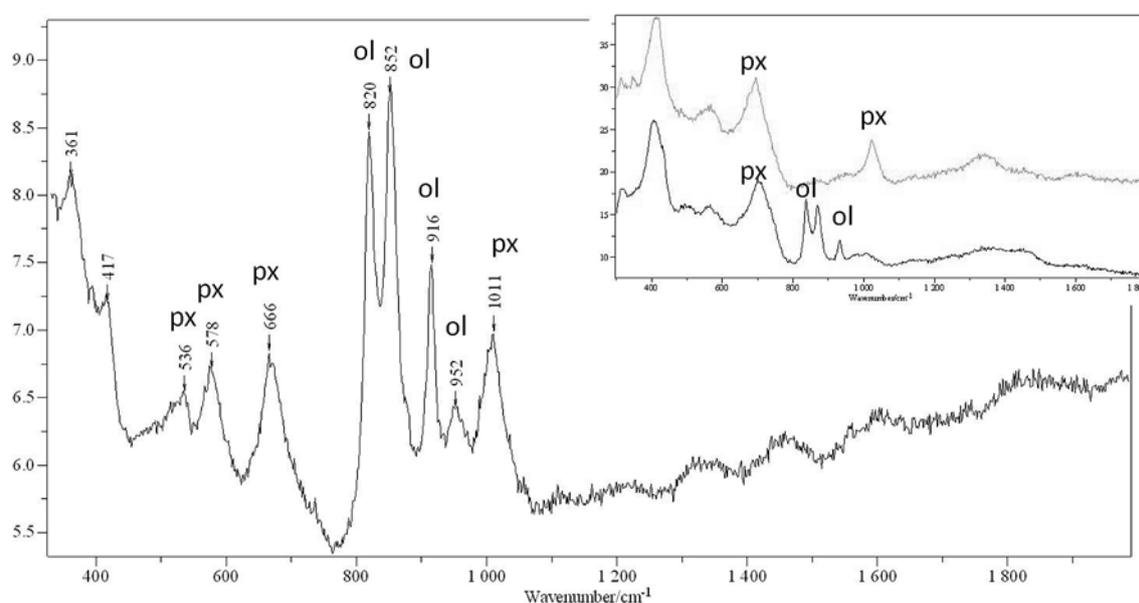
Fig. 4. Three Raman spectra from the shock vein. Spectrum peaks abbreviations: ol-olivine, px-pyroxene.

02500, the shock pressure was too weak to initiate the formation of high-pressure phases. The lack of majorite and ringwoodite in the silicate melt suggests a pressure below 10 GPa, and the absence of plagioclase in the vein assemblage indicates that the pressure was above 2.5 GPa. For data interpretation the Allende phase diagram (Fig. 5) was selected (Agee et al., 1995). The shock veins found in the Sahara 02500 meteorite resemble most closely the shock veins found in the Ramsdorf and Nakhon Pathon L chondrites (Xie et al., 2006), which contain olivine and clinoenstatite indicating a pressure below 15 GPa as they lack high-pressure phases such as majorite and ringwoodite.

6. Conclusions

The Sahara 02500 meteorite experienced an impact in open space. The thermal shock was locally strong enough to make the pyroxene and metal-sulphide phase melt. The melts were super-cooled during rapid quench in the shock veins in a low-gravity environment, which resulted in Ni-rich metal droplets becoming trapped in the recrystallised microcrystalline sub-solidus pyroxene material and the feldspathic glass. The temperature estimates from the micro-granular pyroxene and glass suggest

that the impact had a relatively low energy and that the chondrite experienced moderate (locally strong) shock metamorphism.
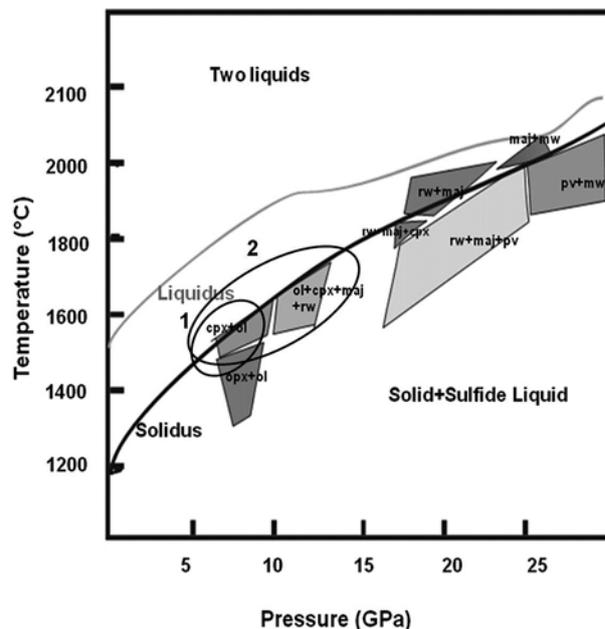

Fig. 5. Crystallisation-pressure regions of the shock-induced melt veins illustrated on a simplified version of the Allende phase diagram (Agee et al., 1995).
1 = Crystallisation region for Sahara 02500 (S4). 2 = Crystallisation region for Ramsdorf (S4) and Nakhon Pathon (S4) (Xie et al., 2006).
Ol = olivine, cpx = clinoenstatite, rw = ringwoodite, maj = majorite, mw = magnesiowüstite, pv = perovskite.

References

Agee, C.B., Li, J., Shannon, M.C. & Circone, S., 1995. Pressure-temperature phase diagram for the Allende meteorite. *Journal of Geophysical Research* 100, 725–740.

Bogert, C.H., Schultz, P.H. & Spray, J.G., 2003. Impact-induced frictional melting in ordinary chondrites: a mechanism for deformation, darkening, and vein formation. *Meteoritics & Planetary Science* 38, 15211531.

Brearley, A.J. & Jones, R.H., 1998. Chondritic meteorites. [In:] J.J. Papike (Ed.): Planetary materials. *Reviews in Mineralogy* 36, 4–90.

Chen, M., El Goresy, A. & Gillet, P., 2004. Ringwoodite lamellae in olivine: clues to olivine-ringwoodite phase transition mechanisms in shocked meteorites and subducting slabs. *Proceedings of the National Academy of Sciences of the USA* 101, 15033–15037.

Lindley, D.H., 1983. Pyroxene thermometry. *American Mineralogist* 68, 477–493.

McDuff, R.E & Ross, E., 2001. Heath phase diagrams and petrological relationships in generation of the ocean crust. www.ocean.washington.edu/oc540/lec01–6/.

Ohtani, E., Kimura, Y., Kimura, M., Takata, T. & Konodo, T., 2004 Formation of high-pressure minerals in shocked L6 chondrite Yamato 791384: constraints on shock conditions and parent body size. *Earth and Planetary Science Letters* 227, 505–515.

Putirka, K.D., 2005. Mantle potential temperatures at Hawaii, Iceland and mid-ocean ridges systems, as inferred from olivine phenocrysts: evidence for thermally driven mantle plumes. *Geochemistry, Geophysics, Geosystems* 6.5, 1–14 (doi:10.1029/2005GC000915).

Rubin, A.E., 1992. A shock-metamorphic model for silicate darkening and compositionally variable plagioclase in CK and ordinary chondrites. *Geochimica et Cosmochimica Acta* 56 17051714.

Rubin, A.E., 2002. Smyer H-chondrite impact-melt breccia and evidence for sulfur vaporization. *Geochimica et Cosmochimica Acta* 66, 699–711.

Stoffler, D., Keil, K. & Scott, E.R.D., 1991. Shock metamorphism of ordinary chondrites. *Geochimica et Cosmochimica Acta* 55, 3845–3867.

Van Schmus, W.R. & Wood, J.A., 1967. A chemical-petrologic classification for the chondritic meteorites. *Geochimica et Cosmochimica Acta* 31, 747–765.

Xie, Z., Sharp, T.G. & De Carli, P.S., 2006a. High-pressure phases in a shock-induced melt vein of the Tenham L6 chondrite: constraints on shock pressure and duration. *Geochimica et Cosmochimica Acta* 70, 504–515.

Xie, Z., Sharp, T.G. & De Carli, P.S., 2006b. Estimating shock pressures based on high-pressure minerals in shock-induced melt veins of L chondrites. *Meteoritics & Planetary Science* 41, 1883–1898.

Xie, X., Sun, Z. & Chen, M., 2011. The distinct morphological and petrological features of shock melt veins in the Suizhou L6 chondrite *Meteoritics & Planetary Science* 46, 459–469.

Yang, C.W., Williams, D.B. & Goldstein, J.I., 1997. A new empirical cooling rate indicator for meteorites based on the size of the cloudy zone of metallic phases. *Meteoritics and Planetary Science* 32, 423–9.